analytical chemistry

pubs.acs.org/ac Article

Enzyme Electrode Biosensors for *N*-Hydroxylated Prodrugs Incorporating the Mitochondrial Amidoxime Reducing Component

Joan Zapiter, Jeffrey R. Harmer, Michel Struwe, Axel Scheidig, Bernd Clement, and Paul V. Bernhardt*

Cite This: *Anal. Chem.* 2022, 94, 9208−9215 Read Online

ACCESS | Metrics & More | Article Recommendations | Supporting Information

ABSTRACT: Human mitochondrial amidoxime reducing component 1 and 2 (mARC1 and mARC2) were immobilised on glassy carbon electrodes using the crosslinker glutaraldehyde. Voltammetry was performed in the presence of the artificial electron transfer mediator methyl viologen, whose redox potential lies negative of the enzymes' $Mo^{VI/V}$ and $Mo^{V/IV}$ redox potentials which were determined from optical spectroelectrochemical and EPR measurements. Apparent Michaelis constants obtained from catalytic limiting currents at various substrate concentrations were comparable to those previously reported in the literature from enzymatic assays. Kinetic parameters for benzamidoxime reduction were determined from cyclic voltammograms simulated using Digisim. pH dependence and stability of the enzyme electrode with time were also determined from limiting catalytic currents in saturating concentrations of benzamidoxime. The same electrode remained active after at least 9 days. Fabrication of this versatile and cost-effective biosensor is effective in screening new pharmaceutically important substrates and mARC inhibitors.

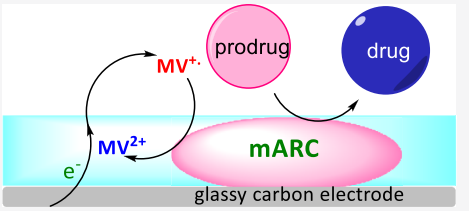

INTRODUCTION

The mitochondrial amidoxime reducing component (mARC) was the fourth and last human enzyme realized to bear a molybdenum cofactor (Moco) along with sulfite oxidase, xanthine oxidase and aldehyde oxidase.[1] mARC is effective in reducing a broad range of *N*-hydroxylated compounds, which may be metabolites from cytochrome P450 and flavin-dependent monooxygenase reactions.[2−5] All mammalian genomes include the *MTARC1* and *MTARC2* genes which produce the paralogues mARC1 and mARC2. mARC1 and mARC2 share approx. 80% sequence similarity (66% identity).[5] While both paralogues are predominantly localised in the outer mitochondrial membrane, tissue-specific expression of mARC1 and mARC2 is different.[6] All Mo enzymes require Moco which is formed through an elaborate, multistep biosynthetic pathway.[7] Breakdowns in this pathway lead to Moco deficiency[8,9] and loss of all four human Mo-enzymes. Moco deficiency is fatal in humans if untreated, principally due to the loss of sulfite oxidase activity and neurological damage caused by toxic sulfite. However, the phenotype for mARC dysfunction, on its own, is unknown.[10]

Amidines and similar highly basic functional groups are present in several drugs and are protonated (charged) at physiological pH which makes drug delivery challenging. Oral bioavailability of amidines can be improved by administering them as amidoxime prodrugs, which are activated by mARC in vivo.[1] Both mARC1 and mARC2 reductively activate the amidoxime anti-cancer drug Upamostat.[10,11] Furthermore, mARC1 and mARC2 may reduce a variety of other *N*-oxygenated compounds such as *N*-hydroxyguanidines, *N*-hydroxysulfonamides, hydroxamic acids, hydroxylamines, *N*-oxides or hydroxyurea.[12] mARC enzymes, along with other molybdoenzymes, are also known to reduce nitrite to NO.[13−15] Recently, mARC2 has been associated with energy metabolism.[16] Also genome-wide association studies have shown a link between a common variant of mARC1 and liver disease.[17−19] Consequently, mARC1 has been proposed as a drug target.[20]

Different from other eukaryotic Mo enzymes, mARC has a small molecular weight (approx. 35 kDa), forms no homodimers, and bears no prosthetic groups other than Moco.[21] Reducing equivalents for substrate turnover are provided by NADH cytochrome b_5 reductase mediated by cytochrome b_5 as part of a three-component enzyme system.[1,4] In mARC, the active site contains a Mo ion coordinated to a pyranopterin dithiolene ligand (molybdopterin), a cysteine residue, an axial oxido group and an equatorial water based ligand that is exchanged with the substrate as shown in Figure 1 as the metal cycles between its active Mo^{IV} and Mo^{VI} oxidation states.[22,23]

The physiological substrate of the mARC enzymes is still unknown. Hence, developing sensors for efficiently screening substrates and new prodrug candidates is important. Recently, a rapid spectrophotometric test based on an NADH assay was developed to screen mARC substrates[24] augmenting earlier studies using HPLC analysis of substrates and products.[25] NADH is a relatively expensive reductant and we have shown

Received: May 24, 2022
Accepted: May 31, 2022
Published: June 14, 2022

https://doi.org/10.1021/acs.analchem.2c02232
Anal. Chem. 2022, 94, 9208−9215

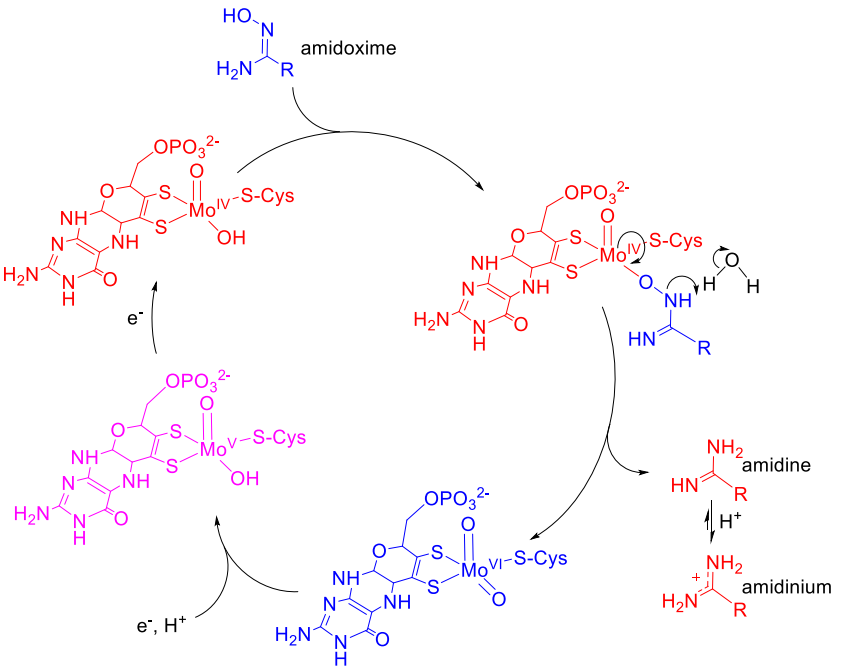

Figure 1. Catalytic cycle for the mARC catalysed reduction of amidoximes.

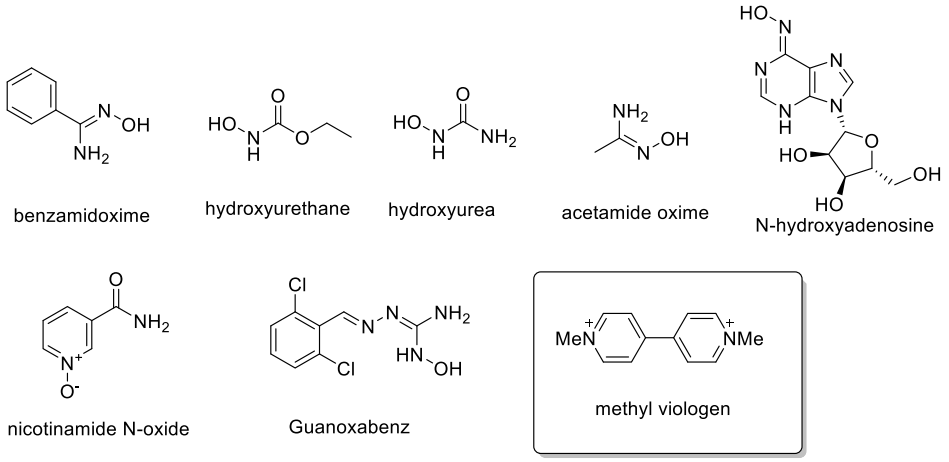

Figure 2. Structures of the mARC substrates examined in this work along with the redox mediator methyl viologen highlighted in the box.

previously that electrochemical methods, as an alternative, can deliver reducing equivalents to drive mARC catalysis utilising cytochrome b_5 as the (native) electron transfer partner between the electrode and the enzyme.[26]

Immobilisation of proteins on electrode surfaces in their active form is crucial in developing stable and practical bioelectrochemical devices for sensing and other biomedical applications.[27] We found that the mARC1:cyt b_5 composite electrode was electro-catalytically active while the proteins were physically entrapped under a dialysis membrane on a chemically modified Au electrode.[26] The stability of the Au:cyt b_5/mARC1 electrode was limited though, and our goal here was to produce a more robust mARC enzyme electrode that could be used for extended periods to screen various substrates of biomedical importance. Also removing the dialysis membrane is desirable to allow efficient substrate mass transport to the immobilised enzyme.[28]

Described herein is a simply constructed electrochemical biosensor for screening mARC1 and mARC2 substrates. Both mARC enzymes were immobilised, separately, on glassy carbon (GC) electrodes by encapsulation in a matrix of glutaraldehyde, a known protein cross-linking agent.[29] All compounds tested using the mARC1 and mARC2 biosensors are listed in Figure 2.

EXPERIMENTAL SECTION

Protein Purification. Human mitochondrial amidoxime reducing component mARC1 and mARC2 were recombinantly expressed in *Escherichia coli* and purified essentially as described by Wahl et al.[21]

Reagents. All reagents and enzyme substrates were obtained commercially. Most experiments were performed in phosphate buffer (100 mM, pH 7) while pH-dependent experiments were carried out with a mixture of citric acid, Bis–Tris, Tris and CHES all at 25 mM and the pH was adjusted by dropwise addition of acetic acid or concentrated NaOH. Ultrapure water with resistivity > 18.2 MΩ·cm was used for all experiments.

https://doi.org/10.1021/acs.analchem.2c02232
Anal. Chem. 2022, 94, 9208−9215

Mo Analysis. The Mo concentration within the mARC enzyme samples was measured using inductively coupled plasma-optical emission spectroscopy following a previously published protocol.[30] The raw data and calibration curves are given in Supporting Information Figure S1.

Spectroelectrochemistry. Optical spectroelectrochemistry of mARC1 and mARC2 (in MES buffer pH 6) was obtained using 1.7 mm path length optically transparent thin layer cell (Pine Instruments) comprising a Pt "honeycomb" working electrode, Pt counter electrode and Ag/AgCl reference electrode. An Ocean Optics USB2000 fibre optic spectrophotometer with a DT-MINI-2-GS miniature deuterium tungsten halogen light source was employed with the spectroelectrochemical cell housed within a Belle Technology anaerobic glove box (O_2 < 20 ppm). Cell potentials were controlled with a Bioanalytical Systems BAS100B/W potentiostat. Absorption data as a function of potential ($A(E)$) were modelled by global analysis of the entire spectra using Reactlab Redox using a 2-electron model to obtain the $Mo^{VI/V}$ and $Mo^{V/IV}$ redox potentials. The relevant equation for this system is given in eq 1 where $A_{Mo(VI)}$, $A_{Mo(V)}$ *and* $A_{Mo(IV)}$ represent the absorbance of each component at that wavelength, *E1* is the $Mo^{VI/V}$ redox potential and *E2* is the $Mo^{V/IV}$ redox potential.

$$A(E) = \frac{A_{Mo(VI)}10^{(E-E1)/59} + A_{Mo(V)} + A_{Mo(IV)}10^{(E2-E)/59}}{1 + 10^{(E-E1)/59} + 10^{(E2-E)/59}} \quad (1)$$

EPR Spectroscopy. X-band (~9.39 GHz) continuous-wave EPR spectra were acquired at 135 K using a Bruker Elexsys E540 spectrometer with Eurotherm temperature control (liquid N_2). The magnetic field was calibrated with 2,2-diphenyl-1-picrylhydrazyl (g = 2.0036). Spectra were measured with a modulation amplitude and frequency of 0.5 mT and 100 kHz, respectively, using a microwave power of 1.262 mW (22 dB of a 200 mW source; non-saturating power condition). Spectral simulation was carried out with the program EasySpin.[31]

The EPR redox titration was carried out in 1 mL of a 51 μM solution of mARC2 in 100 mM MES buffer (pH 6.0). The reductant was sodium dithionite and the oxidant was potassium ferricyanide, each at ca. 10 mM concentration and added in small aliquots (<1 μL). The redox mediators 2,6-dimethylbenzoquinone, 2,5-dihydroxybenzoquinone, potassium indigo-5,5′-7-trisulfonate, 2-hydroxynaphthoquinone, sodium anthraquinone-2-sulfonate and Safranin T were used to buffer the oxidation reduction potential (ORP). All manipulations were carried out in a Belle Technology anaerobic glovebox (O_2 < 20 ppm). The ORP was measured after ca. 15 min Equilibration time using a Jenco 6230 N meter and Pt/Ag−AgCl combination electrode calibrated with quinhydrone (E′ +285 mV vs the normal hydrogen electrode (NHE) at pH 7 and 298 K). Each sample comprised a 50 μL aliquot that was transferred to each EPR tube within the glovebox, sealed then frozen immediately upon removal from the glovebox.

The ORP (E)-dependent Mo^V EPR intensity data ($I(E)$) were fit to eq 2, a simplified version of eq 1, which applies for a system such as this where the single electron reduced form is the only signal giving species. Again *E1* is the $Mo^{VI/V}$ redox potential and *E2* is the $Mo^{V/IV}$ potential and I_{max} is the maximum EPR intensity of the Mo^V form.

$$I(E) = \frac{I_{max}}{1 + 10^{(E-E1)/59} + 10^{(E2-E)/59}} \quad (2)$$

Electrochemistry. *Enzyme Electrode Preparation.* GC electrodes (3.0 mm diameter) were obtained from Bioanalytical Systems Inc. Cleaning involved mechanical polishing with alumina, rinsing with water and absolute ethanol then drying under N_2. A mixture of 3.5 μL of mARC1 (260 μM) or mARC2 (197 μM) and 2 μL of 0.25% glutaraldehyde in water was then applied to an inverted electrode and evaporated to a film for 3−4 h at 4 °C.

Cyclic Voltammetry. Electrochemical measurements were obtained using a BAS100B/W potentiostat using a standard three-electrode cell comprised of a GC working electrode, Ag/AgCl reference electrode (calibrated with quinhydrone as described above) and a Pt wire auxiliary electrode. All potentials are referenced against NHE. Solutions were deoxygenated with N_2 for at least 10 min prior to analysis and kept under a blanket of N_2 thereafter. Voltammograms for pH-dependence studies were obtained with an electrode covered by a dialysis membrane (MW cut-off 3500 Da), as described previously.[32] All experiments were conducted at room temperature (298 K).

Apparent Michaelis constants ($K_{M,app}$) for each substrate, S, were determined from the limiting catalytic currents at low potential for different substrate concentrations according to eq 3

$$i_{lim} = \frac{i_{max}[S]}{K_{M,app} + [S]} \quad (3)$$

For pH dependence studies, CVs of mARCs 1 and 2 on GC with glutaraldehyde were measured in the presence of a saturating amount of benzamidoxime (2.4 mM) in 100 mM mixed buffer at different pHs. Variation of the bell-shaped catalytic current profile (i_{max}) with pH was modelled with eq 4.[33] Here pK_{a_1} coincides with a deprotonation reaction at the active site that turns off catalysis while pK_{a_2} is a protonation reaction that also stops catalysis and i_{opt} is the limiting current at the pH optimum.

$$i_{max} = \frac{i_{opt}}{1 + 10^{(pH-pK_{a_1})} + 10^{(pK_{a_2}-pH)}} \quad (4)$$

Electrochemical Simulations. The electrochemical kinetic model describing mediated mARC catalysis is shown in Scheme 1 with all relevant rate constants defined. Simulations

Scheme 1. Electrochemical Kinetic Model for Mediated Catalysis of mARC which Is Shown in Its Three Oxidation States Mo^{VI}, Mo^V and Mo^{IV}

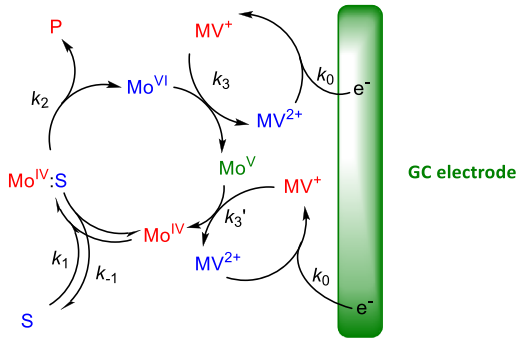

https://doi.org/10.1021/acs.analchem.2c02232
Anal. Chem. 2022, 94, 9208−9215

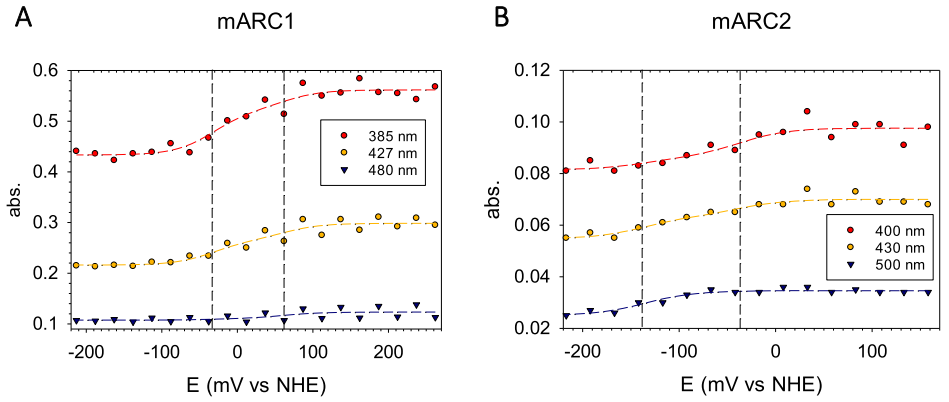

Figure 3. Measured (symbols) and calculated (broken curves) absorbances at different wavelengths as a function of potentials for (A) mARC1 and (B) mARC2 in 20 mM MES pH 6. The $Mo^{VI/V}$ and $Mo^{V/IV}$ redox potentials are marked with the vertical broken lines.

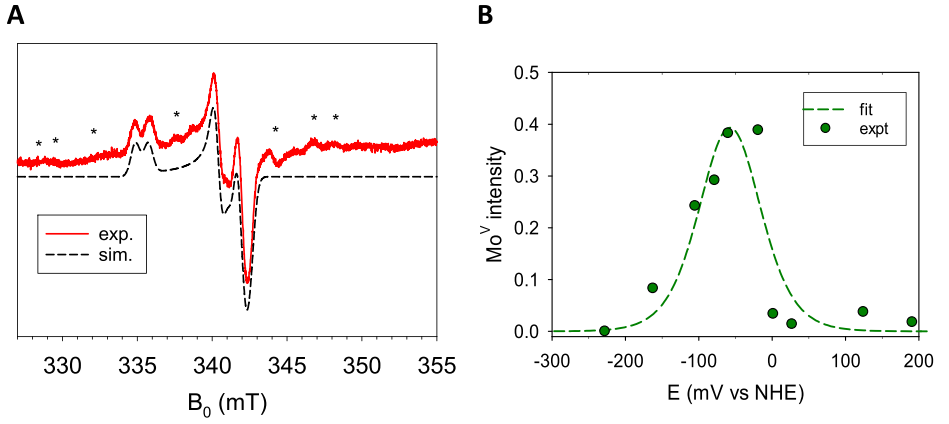

Figure 4. (A) X-band (~9.39 GHz) 135 K EPR spectrum of mARC2 poised at −29 mV versus NHE (red solid line) and simulated spectrum (broken line) with g_1 2.0015 (A_1 24 MHz); g_2 1.967 (A_2 40.6 MHz); g_3 1.9623 (A_3 27.6 MHz). Hyperfine coupling to the minor ^{95}Mo and ^{97}Mo isotopes is indicated with asterisks but not modelled in the simulation. (B) Mo^V EPR signal intensity as a function of redox potential. The broken curve is the fit to eq 2 with $Mo^{VI/V}$ and $Mo^{V/IV}$ redox potentials −40(±20) and −92(±20) mV versus NHE, respectively.

of all cyclic voltammograms (CVs) were performed using Digisim version 3.03b.[34] The electrode surface area and the double-layer capacitance were 0.055 cm^2 and 10−20 μF (depending on the enzyme electrode preparation), respectively. For the mediator and substrate, semi-infinite diffusion was assumed, while a finite diffusion (blocked boundary) model was used for the surface-confined mARC enzyme. All pre-equilibration reactions were disabled. The redox potential and diffusion coefficients of methyl viologen in its oxidised and reduced forms was determined from control voltammetry experiments in the absence of enzyme or substrate. Diffusion coefficients for the enzymes and substrates were 1.0×10^{-8} and 1.0×10^{-5} cm^2 s^{-1}, respectively, and held constant for all simulations. Kinetic parameters for the enzyme/substrate dependent reactions (k_1/k_{-1} and k_2) were determined for sets of experiments with different substrate concentrations and scan rates. Outer sphere electron transfer rate constants of the Mo^{VI} (k_3) and Mo^V (k_3') states of mARC with methyl viologen were assumed to be equal. The catalytic waveforms were consistent with a single electron transfer reaction between the mediator and enzyme, that is $MV^{+\bullet}$ is the electron donor to the mARC enzyme. All model parameters and fitting protocols are assembled in the Supporting Information (pp S13−S14).

RESULTS AND DISCUSSION

Redox Potentials of mARC1 and mARC2. *Optical Spectroelectrochemistry.* Figure 3 shows a collection of single wavelength absorption profiles as a function of redox potential for mARC1 and mARC2. The raw data are in the Supporting Information. As previously reported,[21,35] the spectra of the oxidized and reduced forms of mARC are rather featureless comprising broad shoulders in the range 380−550 nm. Small but reversible changes in the spectra of mARC1 and mARC2 were identified as a function of potential which enabled the $Mo^{VI/V}$ and $Mo^{V/IV}$ redox potentials to be calculated with Reactlab Redox (eq 1) and these are indicated by the vertical broken lines in Figure 3A,B which coincide with inflexion points on the curves. The respective $Mo^{VI/V}$ and $Mo^{V/VI}$ redox potentials of mARC1 were determined to be +64(±10) and −30(±10) mV versus NHE at pH 6, while for mARC2, these potentials were significantly lower at −37(±10) and −137(±10) mV versus NHE.

EPR Spectroscopy. The EPR spectra of mARC1 and mARC2 in their intermediate Mo^V oxidation state have been reported previously.[21,36] The spectrum of mARC2 poised at −29 mV versus NHE by chemical reduction with a set of redox mediators (see Experimental Section) is shown in Figure 4A which exhibits axial symmetry and a large proton hyperfine coupling to the equatorial hydroxido ligand. The simulated spectrum is also shown next to the experimental spectrum.

https://doi.org/10.1021/acs.analchem.2c02232
Anal. Chem. 2022, 94, 9208−9215

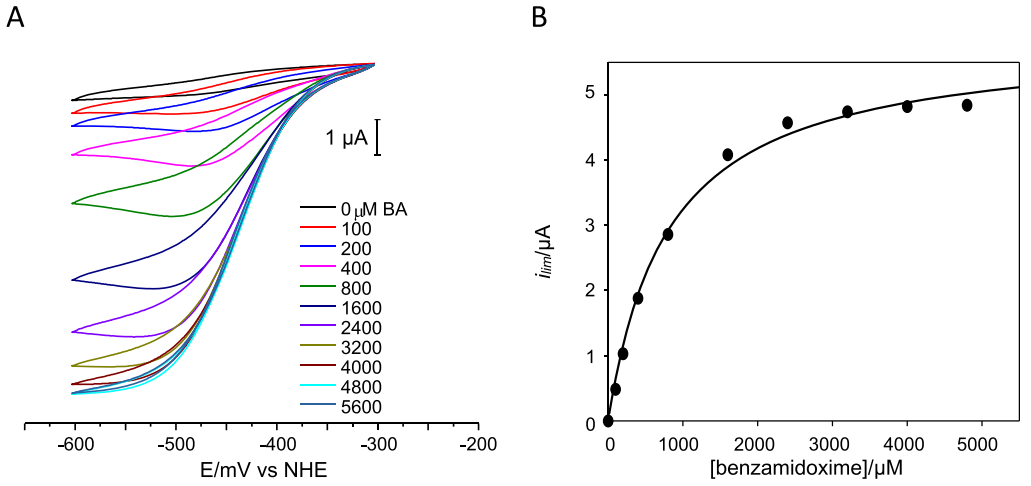

Figure 5. (A) CVs of MV^{2+} (40 μM) at the GC/glutaraldehyde-mARC1 electrode at different benzamidoxime (BA) concentrations, and (B) plot of the maximum current at −500 mV as a function of BA concentration. The solid line is a fit to eq 3 with $K_{M,app}$ = 810 μM. Scan rate is 5 mV s^{-1} in 100 mM phosphate buffer (pH 7).

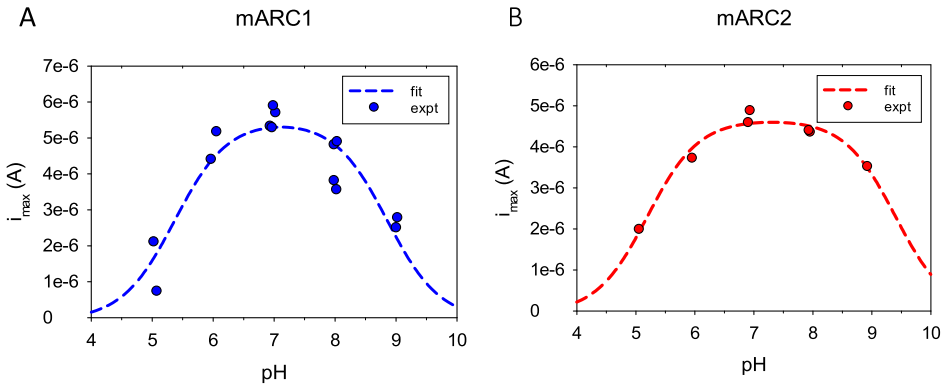

Figure 6. pH profiles for the limiting cathodic current for (A) GC/mARC1 and (B) GC/mARC2 in the presence of 2.4 mM benzamidoxime and 40 μM methyl viologen in 100 mM mixed buffer (citric acid, Bis−Tris, Tris and CHES each 25 mM).

Satellite peaks from ^{95}Mo and ^{97}Mo hyperfine coupling (I = 5/2, total isotopic abundance ∼ 24%) are marked with an asterisk, but due to their weak intensity they were not included in the simulation.

A redox titration was carried out where the intensity of the EPR active Mo^{V} form rose and then fell as the potential was lowered. All potential dependent spectra appear in the Supporting Information (Figure S3). The results are summarised in Figure 4B. From this analysis (eq 2), the $Mo^{VI/V}$ and $Mo^{V/IV}$ redox potentials of mARC2 were −40(±20) and −92(±20) mV versus NHE which agrees with the optical spectroelectrochemistry data. Precipitation of mARC1 during the redox titration prevented an EPR redox titration being conducted on this enzyme.

Catalytic Voltammetry Mediated by Methyl Viologen. *Benzamidoxime Reduction.* An effective redox mediator to drive mARC catalysis should have a redox potential significantly more negative than the enzyme. Methyl viologen is a suitable candidate, which typically shows reversible single electron electrochemistry at a low potential. Figure 5A shows a series of CVs of methyl viologen (MV^{2+}) at the CG/mARC1 electrode, with the enzyme immobilised as part of a glutaraldehyde-crosslinked film, at different concentrations of benzamidoxime (BA). As the concentration of BA increases, the original symmetrical, reversible CV for $MV^{2+/+\bullet}$ (−436 mV vs NHE) transforms into an asymmetric cathodic peak which then becomes sigmoidal at high (saturating) concentrations of BA. The increase in current with BA concentration is due to the larger amount of substrate being reduced, which consequently produces more MV^{2+} at the electrode surface as the product of substrate reduction. The CVs also approach a more sigmoidal form with increasing BA concentration, which is typical of an electrochemical steady state.

Eventually the catalytic current reaches a plateau as the enzyme becomes saturated with substrate. A plot of limiting currents at −500 mV (vs NHE) against concentration of benzamidoxime (Figure 5B) follows Michaelis−Menten kinetics (eq 3) and an apparent Michaelis constant ($K_{M,app}$) was obtained for benzamidoxime catalysed reduction by mARC1 of 810 μM. Caution should be taken when comparing these constants with somewhat lower K_M values measured from biochemical assays, which use cytochrome b_5 and NADH reductase,[10,21,37,38] as the currents here are not only determined by enzyme turnover but also the mARC/$MV^{+\bullet}$ reaction depending on the conditions. This will be revisited when considering the electrochemical simulations.

The corresponding CVs and K_M plot obtained for the GC/glutaraldehye-mARC2 electrode are shown in Figure S4 (Supporting Information). Analogously to the mARC1 isoform, the mARC2-modified electrode was able to catalyse BA reduction as evidenced by the increasing reductive currents and sigmoidal CVs at higher substrate concentrations. The

https://doi.org/10.1021/acs.analchem.2c02232
Anal. Chem. 2022, 94, 9208−9215

Table 1. $K_{M,app}$ and i_{max} Values (eq 3) for Different mARC1 and mARC2 Substrates Determined Electrochemically (40 mV MV^{2+}, 100 mM Phosphate Buffer pH 7)[a]

	mARC1		mARC2	
substrate	$K_{M,app}/\mu M$	$i_{max}/\mu A$	$K_{M,app}/\mu M$	$i_{max}/\mu A$
acetamide oxime	$1.7(3) \times 10^3$	$1.1(1) \times 10^1$	$1.3(2) \times 10^3$	4.6(2)
benzamidoxime	$8.1(7) \times 10^2$	5.9(2)	$1.1(1) \times 10^3$	3.1(1)
guanoxabenz	$6(1) \times 10^2$	2.1(1)	$9(2) \times 10^2$	1.5(1)
hydroxyurea	$5.8(5) \times 10^2$	3.1(1)	$6(2) \times 10^2$	$4.0(4) \times 10^{-1}$
N-hydroxyadenosine	$4.4(8) \times 10^2$	1.6(1)	$3.0(4) \times 10^2$	$7.7(3) \times 10^{-1}$
N-hydroxyurethane	$5.9(6) \times 10^2$	3.7(1)	$3.0(7) \times 10^2$	$4.9(3) \times 10^{-1}$
nicotinamide *N*-oxide	$3.9(5) \times 10^2$	1.5(1)	$1.9(4) \times 10^2$	$1.5(1) \times 10^{-1}$

[a]The errors in the last significant figure are from non-linear fits of the data to eq 3.

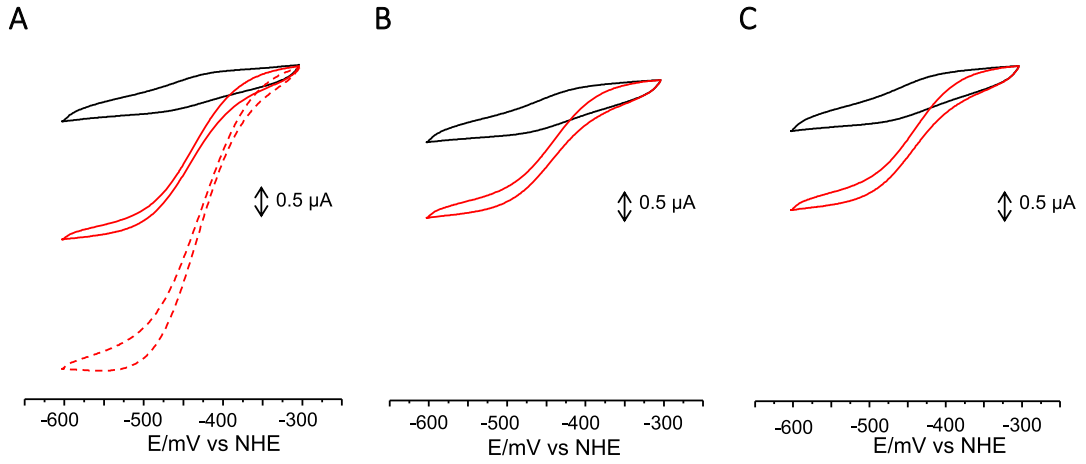

Figure 7. CVs of 40 μM methyl viologen at the GC/glutaraldehyde-mARC1 electrode on (A) day 1, (B) day 4 and (C) day 9 before (black) and after (red) addition of 2400 μM benzamidoxime (BA). In panel (A) the broken curve is the first run and the solid curve is the second run after testing multiple substrates (as in Figure S18). Scan rate is 5 mV s^{-1} in 100 mM phosphate buffer pH 7.

apparent Michaelis constant was comparable to previously reported data.[37]

pH Dependence. Electrode-immobilised mARC1 and mARC2 both catalyse the reduction of BA but the limiting current is pH dependent (Figures 6 and S5A,B). This is also consistent with results published for membrane-bound mARC1 on gold electrodes modified with self-assembled monolayers of alkyl thiols and chitosan.[26] The dependence of i_{max} at −500 mV versus NHE with pH was modelled with eq 4 as shown in Figure 6 where bell-shaped profiles were found. From eq 4 protonation constants were obtained that are associated with acid base equilibria that switch off catalysis. For mARC1, pK_{a1} = 8.9 (deprotonation) and pK_{a2} = 5.4 (protonation) while for mARC2, pK_{a1} = 9.5 and pK_{a2} = 5.1.

Other Substrates. Reduction of other substrates shown in Figure 2 was investigated using the GC/glutaraldehyde-mARC1 and GC/glutaraldehyde-mARC2 electrodes. CVs and plots from which the apparent Michaelis constant, $K_{M,app}$, were obtained for each substrate are shown in the Supporting Information (Figures S6−S17). The $K_{M,app}$ values summarized on Table 1 are as expected,[24,39] except for higher previously reported values for *N*-hydroxyadenosine.[25] However, these apparent K_M values should not be directly compared with those measured by biochemical assays due to the rate of $MV^{+\cdot}$ reduction also being a kinetic factor.

Electrode Stability. Utilising our previously published protocol comprising a thiol-modified Au electrode with cytochrome b_5 and mARC1,[26] we found that catalytic activity was lost if the enzyme was transferred between solutions. Long-term stability of the GC/glutaraldehyde-mARC1 electrode was far superior. As shown in Figure 7A, the catalytic current from a freshly prepared electrode in the presence of a saturating concentration of BA (broken line) decreased to approximately half within a couple of hours (red solid line).

However, after that initial decrease the catalytic current was effectively constant over the next 9 days if the electrode was stored in buffer at 5 °C (Figure 7B,C). The initial sharp decrease in activity is likely due to dissociation of loosely bound mARC from the electrode surface, while the remaining activity is due to mARC entrapped within the glutaraldehyde crosslinked film. Another ideal feature of this enzyme electrode is that it may be transferred between solutions containing different (potential) substrates for screening. This is illustrated in Figure S18 where catalytic CVs of the GC/glutaraldehyde-mARC1 electrode were obtained initially with *N*-hydroxyadenosine (Figure S18A). Washing the electrode in fresh buffer and transferring to 40 μM MV^{2+} solutions containing *N*-hydroxyurethane (Figure S18B) then guanoxabenz (Figure S18C) demonstrate that the electrode's catalytic activity is preserved.

Methyl Viologen Concentration Dependence. In the absence of MV^{2+} no catalysis is seen at either the GC/glutaraldehyde-mARC1 or GC/glutaraldehyde-mARC2 electrodes when BA is added. This confirms that direct electron transfer with the enzyme does not occur under these conditions, which was also found in our previous study using a chemically modified Au electrode.[26] As the MV^{2+} concentration increases, a sigmoidal wave emerges (Figure

https://doi.org/10.1021/acs.analchem.2c02232
Anal. Chem. 2022, 94, 9208−9215

S19), which eventually becomes peak shaped as the concentration of mediator at the electrode surface becomes too great to maintain the electrochemical steady state. Importantly, only low concentrations of MV^{2+} (~20−40 μM) are required, and are desirable, to elicit a strong catalytic current response.

Electrochemical Simulations. Kinetic parameters for benzamidoxime reduction catalysis (Scheme 1) were determined by electrochemical simulation, which involves fitting the experimental data collected at different concentrations of substrate (BA) and mediator (MV^{2+}) over a range of sweep rates. The most important data are summarised in Table 2

Table 2. Kinetic Parameters Generated from Digisim Simulations for GC/mARC-Glutaraldehyde with Benzamidoxime as Substrate[a]

	mARC1	mARC2
k_1 (M^{-1} s^{-1})	5.0×10^3	1.7×10^3
k_{-1} (s^{-1})	2.5×10^{-3}	1.2×10^{-2}
k_2 (s^{-1})	2.0	2.0
k_{-2} (M^{-1} s^{-1})	*2.0×10^{-5}*	*1.1×10^{-5}*
$k_3 = k_3'$ (M^{-1} s^{-1})	1.5×10^4	1.8×10^4
$k_{-3} = k_{-3}'$ (M^{-1} s^{-1})	*1.5×10^{-1}*	*1.8×10^{-1}*

[a]Numbers in italics are approximate and have no significant effect on the simulations. They may be taken as upper bounds. The estimated error on these parameters is ±20%.

while remaining parameters may be found in the Supporting Information (p S13). Some examples of the experimental and simulated CV data for mARC1 and mARC2 are shown in Figures S20−S24 where the concentrations of BA and MV^{2+} are varied as well as the scan rate.

There is a sloping baseline in the experimental data that is not modelled by the simulations. As the BA concentration increases (Figure S20A−D) the CVs first become asymmetric as the anodic peak diminishes and the cathodic peak increases in intensity. Under these conditions mass transport of BA to the enzyme is rate limiting. At the faster scan rates (30, 50 mV s^{-1}) the anodic peak persists due to heterogeneous electron transfer (k_0) being faster than homogeneous electron transfer (k_3, k_3'). Finally at saturating BA concentrations (Figure S20D) all CVs take on a sigmoidal waveform and the limiting currents (corrected for charging current) are almost the same which is indicative of the reaction being enzyme limited.

CONCLUSIONS

The present results have shown that a versatile and simply prepared enzyme electrode can be constructed to examine potential mARC1 and mARC2 substrates that may provide viable *N*-hydroxylated prodrugs. The physiological substrates for mARC1 and mARC2 remain unknown while the physiological targets for the bacterial mARC homologues YiiM and YcbX, which show similarly broad-spectrum activity,[30,40] are believed to be cytotoxic and mutagenic *N*-hydroxylated purines (such as *N*-hydroxyadenosine, Figure 2). The quest to better understand the physiology and pharmacology of the human mARC enzymes will be enhanced by further methods, like this, to rapidly screen substrates and inhibitors of enzyme activity.

ASSOCIATED CONTENT

Supporting Information

The Supporting Information is available free of charge at https://pubs.acs.org/doi/10.1021/acs.analchem.2c02232.

(PDF)

AUTHOR INFORMATION

Corresponding Author

Paul V. Bernhardt − *School of Chemistry and Molecular Biosciences, The University of Queensland, Brisbane 4072, Australia;* orcid.org/0000-0001-6839-1763; Email: p.bernhardt@uq.edu.au

Authors

Joan Zapiter − *School of Chemistry and Molecular Biosciences, The University of Queensland, Brisbane 4072, Australia*

Jeffrey R. Harmer − *Centre for Advanced Imaging, The University of Queensland, Brisbane 4072, Australia;* orcid.org/0000-0003-4583-2401

Michel Struwe − *Pharmazeutisches Institut, Universität Kiel, Kiel 24118, Germany; Zoologisches Institut/Strukturbiologie, Kiel 24118, Germany*

Axel Scheidig − *Zoologisches Institut/Strukturbiologie, Kiel 24118, Germany*

Bernd Clement − *Pharmazeutisches Institut, Universität Kiel, Kiel 24118, Germany;* orcid.org/0000-0003-1412-6117

Complete contact information is available at: https://pubs.acs.org/10.1021/acs.analchem.2c02232

Author Contributions

The manuscript was written through contributions of all authors. All authors have given approval to the final version of the manuscript.

Notes

The authors declare no competing financial interest.

ACKNOWLEDGMENTS

Financial support from the Australian Research Council (DP190103158 to P.V.B.) and The University of Queensland for an International Postgraduate Research Scholarship (to J.Z.) is gratefully acknowledged.

REFERENCES

(1) Havemeyer, A.; Bittner, F.; Wollers, S.; Mendel, R.; Kunze, T.; Clement, B. *J. Biol. Chem.* **2006**, *281*, 34796−34802.
(2) Foti, R. S.; Dalvie, D. K. *Drug Metab. Dispos.* **2016**, *44*, 1229.
(3) Hlavica, P. *Drug Metab. Rev.* **2002**, *34*, 451−477.
(4) Plitzko, B.; Havemeyer, A.; Bork, B.; Bittner, F.; Mendel, R.; Clement, B. *Drug Metab. Dispos.* **2016**, *44*, 1617−1621.
(5) Ott, G.; Havemeyer, A.; Clement, B. *J. Biol. Inorg Chem.* **2015**, *20*, 265−275.
(6) Ahire, D.; Basit, A.; Christopher, L. J.; Iyer, R.; Leeder, J. S.; Prasad, B. *Drug Metab. Dispos.* **2021**, *50*, 191.
(7) Mendel, R. R.; Leimkühler, S. *J. Biol. Inorg Chem.* **2015**, *20*, 337−347.
(8) Atwal, P. S.; Scaglia, F. *Mol. Genet. Metab.* **2016**, *117*, 1−4.
(9) Reiss, J.; Hahnewald, R. *Hum. Mutat.* **2011**, *32*, 10−18.
(10) Ott, G.; Reichmann, D.; Boerger, C.; Cascorbi, I.; Bittner, F.; Mendel, R.-R.; Kunze, T.; Clement, B.; Havemeyer, A. *Drug Metab. Dispos.* **2014**, *42*, 718−725.
(11) Froriep, D.; Clement, B.; Bittner, F.; Mendel, R. R.; Reichmann, D.; Schmalix, W.; Havemeyer, A. *Xenobiotica* **2013**, *43*, 780−784.

(12) Indorf, P.; Kubitza, C.; Scheidig, A. J.; Kunze, T.; Clement, B. *J. Med. Chem.* **2020**, *63*, 6538−6546.
(13) Bender, D.; Schwarz, G. *FEBS Lett.* **2018**, *592*, 2126−2139.
(14) Llamas, A.; Chamizo-Ampudia, A.; Tejada-Jimenez, M.; Galvan, A.; Fernandez, E. *BioFactors* **2017**, *43*, 486−494.
(15) Yang, J.; Giles, L. J.; Ruppelt, C.; Mendel, R. R.; Bittner, F.; Kirk, M. L. *J. Am. Chem. Soc.* **2015**, *137*, 5276−5279.
(16) Rixen, S.; Havemeyer, A.; Tyl-Bielicka, A.; Pysniak, K.; Gajewska, M.; Kulecka, M.; Ostrowski, J.; Mikula, M.; Clement, B. *J. Biol. Chem.* **2019**, *294*, 17593−17602.
(17) Emdin, C. A.; Haas, M. E.; Khera, A. V.; Aragam, K.; Chaffin, M.; Klarin, D.; Hindy, G.; Jiang, L.; Wei, W.-Q.; Feng, Q.; Karjalainen, J.; Havulinna, A.; Kiiskinen, T.; Bick, A.; Ardissino, D.; Wilson, J. G.; Schunkert, H.; McPherson, R.; Watkins, H.; Elosua, R.; Bown, M. J.; Samani, N. J.; Baber, U.; Erdmann, J.; Gupta, N.; Danesh, J.; Saleheen, D.; Chang, K.-M.; Vujkovic, M.; Voight, B.; Damrauer, S.; Lynch, J.; Kaplan, D.; Serper, M.; Tsao, P.; Mercader, J.; Hanis, C.; Daly, M.; Denny, J.; Gabriel, S.; Kathiresan, S.; Kathiresan, S. *PLoS Genet.* **2020**, *16*, No. e1008629.
(18) Schneider, C. V.; Schneider, K. M.; Conlon, D. M.; Park, J.; Vujkovic, M.; Zandvakili, I.; Ko, Y.-A.; Trautwein, C.; Carr, R. M.; Strnad, P.; Thaiss, C. A.; Rader, D. J.; Rader, D. J. *Med* **2021**, *2*, 851−863.
(19) Janik, M. K.; Smyk, W.; Kruk, B.; Szczepankiewicz, B.; Górnicka, B.; Lebiedzińska-Arciszewska, M.; Potes, Y.; Simões, I. C. M.; Weber, S. N.; Lammert, F.; Więckowski, M. R.; Milkiewicz, P.; Krawczyk, M. *Sci. Rep.* **2021**, *11*, 24407.
(20) Haas, M. E.; Pirruccello, J. P.; Friedman, S. N.; Wang, M.; Emdin, C. A.; Ajmera, V. H.; Simon, T. G.; Homburger, J. R.; Guo, X.; Budoff, M.; Corey, K. E.; Zhou, A. Y.; Philippakis, A.; Ellinor, P. T.; Loomba, R.; Batra, P.; Khera, A. V. *Cell Genomics* **2021**, *1*, 100066.
(21) Wahl, B.; Reichmann, D.; Niks, D.; Krompholz, N.; Havemeyer, A.; Clement, B.; Messerschmidt, T.; Rothkegel, M.; Biester, H.; Hille, R.; Mendel, R. R.; Bittner, F. *J. Biol. Chem.* **2010**, *285*, 37847−37859.
(22) Havemeyer, A.; Lang, J.; Clement, B. *Drug Metab. Rev.* **2011**, *43*, 524−539.
(23) Kubitza, C.; Bittner, F.; Ginsel, C.; Havemeyer, A.; Clement, B.; Scheidig, A. J. *Proc. Natl. Acad. Sci. U.S.A.* **2018**, *115*, 11958−11963.
(24) Indorf, P.; Kubitza, C.; Scheidig, A. J.; Kunze, T.; Clement, B. *J. Med. Chem.* **2020**, *63*, 6538−6546.
(25) Krompholz, N.; Krischkowski, C.; Reichmann, D.; Garbe-Schönberg, D.; Mendel, R.-R.; Bittner, F.; Clement, B.; Havemeyer, A. *Chem. Res. Toxicol.* **2012**, *25*, 2443−2450.
(26) Kalimuthu, P.; Havemeyer, A.; Clement, B.; Kubitza, C.; Scheidig, A. J.; Bernhardt, P. V. *Electrochem. Commun.* **2017**, *84*, 90−93.
(27) Guisan, J. M.; Bolivar, J. M.; López-Gallego, F.; Rocha-Martín, J. *Immobilization of Enzymes and Cells: Methods and Protocols*. 4th ed.; Humana Press: New York, NY, 2020.
(28) Kalimuthu, P.; Kappler, U.; Bernhardt, P. V. *J. Phys. Chem. B* **2014**, *118*, 7091−7099.
(29) Barbosa, O.; Ortiz, C.; Berenguer-Murcia, Á.; Torres, R.; Rodrigues, R. C.; Fernandez-Lafuente, R. *RSC Adv.* **2014**, *4*, 1583−1600.
(30) Kalimuthu, P.; Harmer, J. R.; Baldauf, M.; Hassan, A. H.; Kruse, T.; Bernhardt, P. V. *Biochim. Biophys. Acta* **2022**, *1863*, 148523.
(31) Stoll, S.; Schweiger, A. *J. Magn. Reson.* **2006**, *178*, 42−55.
(32) Kalimuthu, P.; Fischer-Schrader, K.; Schwarz, G.; Bernhardt, P. V. *J. Phys. Chem. B* **2013**, *117*, 7569−7577.
(33) Brody, M. S.; Hille, R. *Biochemistry* **1999**, *38*, 6668−6677.
(34) Rudolf, M.; Feldberg, S. W. *DigiSim* Version 3.03b; Bioanalytical System: West Lafayette, 2004.
(35) Wang, J.; Keceli, G.; Cao, R.; Su, J.; Mi, Z. *Redox Rep.* **2017**, *22*, 17−25.
(36) Rajapakshe, A.; Astashkin, A. V.; Klein, E. L.; Reichmann, D.; Mendel, R. R.; Bittner, F.; Enemark, J. H. *Biochemistry* **2011**, *50*, 8813−8822.
(37) Kotthaus, J.; Wahl, B.; Havemeyer, A.; Kotthaus, J.; Schade, D.; Garbe-Schönberg, D.; Mendel, R.; Bittner, F.; Clement, B. *Biochem. J.* **2011**, *433*, 383−391.
(38) Bauch, E.; Reichmann, D.; Mendel, R.-R.; Bittner, F.; Manke, A.-M.; Kurz, P.; Girreser, U.; Havemeyer, A.; Clement, B. *ChemMedChem* **2015**, *10*, 360−367.
(39) Ginsel, C.; Plitzko, B.; Froriep, D.; Stolfa, D. A.; Jung, M.; Kubitza, C.; Scheidig, A. J.; Havemeyer, A.; Clement, B. *Drug Metab. Dispos.* **2018**, *46*, 1396−1402.
(40) Kozmin, S. G.; Leroy, P.; Pavlov, Y. I.; Schaaper, R. M. *Mol. Microbiol.* **2008**, *68*, 51−65.

https://doi.org/10.1021/acs.analchem.2c02232
Anal. Chem. 2022, 94, 9208−9215